WEP Warwick Evans Publishing

International Journal of Mechanical and Electrical Engineering

ISSN: 3005-9615 (Print), ISSN: 3005-7132 (Online) | Volume 2, Number 2, Year 2024
DOI: https://doi.org/10.62051/ijmee.v2n2.09
Journal homepage: https://wepub.org/index.php/IJMEE/index

# Harmonic Interaction Analysis of Inverters Based on Harmonic State-Space Model Considering Dead-Zone Effect

Shangshang Li *, Shiyu Wang, Yuxuan Mao

School of Electrical Engineering and Automation, Henan Polytechnic University, Jiaozuo 454003, China

* Corresponding Author: Shangshang Li

## ABSTRACT

In the context of increasing device switching frequencies year by year, non-ideal factors such as dead-zone effects in inverters not only cause output waveform distortion, but also generate harmonics that make the interaction between inverters and power grids more complex. In order to accurately describe and analyze this phenomenon and establish a more practical grid-connected inverter model, this paper proposes and establishes a three-phase LCL grid-connected inverter harmonic state space model that considers dead-zone effects. By incorporating dead-zone effects into the modeling process, the system transfer function matrix is derived to quantify the harmonic interaction coefficient between the inverter and the power grid, and the influence mechanism of dead-zone effects on the harmonic interaction process at high switching frequencies is analyzed in depth. The necessity of considering dead-zone effects is illustrated through simulation, and the effectiveness and accuracy of the inverter HSS model considering the effects of dead-zone effects are verified through experiments.

## KEYWORDS

Inverter; Harmonic State Space; Dead-zone Effects; Harmonic Interaction.

## 1. INTRODUCTION

In recent years, the power system has exhibited 'dual high' characteristics, with a high proportion of new energy and power electronic devices. The power grid employs a large number of inverters, power electronic devices, nonlinear loads, and impulse loads, leading to increasingly complex harmonic interaction problems [1, 2]. To ensure the stable operation of the power grid, it is necessary to establish accurate mathematical analysis models, conduct in-depth research on harmonic interaction processes, and reveal their interaction mechanisms.

Mathematical analysis models are mainly divided into two categories: single frequency models and multi frequency models [3]. The single frequency model modeling method is simple and feasible, but it only describes the relationship between input and output components of the same frequency in the system, and cannot accurately reflect the mechanism of harmonic interaction. The multi frequency model can accurately describe the interaction between input and output components of multiple frequencies in the system. The Harmonic State Space (HSS) model, as a type of multi frequency model, is a linear time period (LTP) model [4, 5]. It characterizes the input and output signals in the form of finite harmonic components, and converts the periodic variables in the time domain into constants in the frequency domain through Fourier series. A linear time invariant (LTI) model with multiple inputs and multiple outputs is established in the frequency domain. Therefore, it can

accurately reflect the interaction relationship between the input and output components of the inverter system at different frequencies.

At present, the HSS model has been applied in power electronic equipment such as grid connected inverters, DC/DC converters, and MMC. Reference [6, 7] uses the HSS model to derive the harmonic transfer function matrix of multi input multi output systems, and analyzes the harmonic interaction mechanism between the grid connected inverter system and the power grid system as a multi input multi output system. On the basis of establishing a HSS model for single-phase grid connected inverters, reference [8] shifted the research perspective from studying the "external interaction" between the inverter and the power grid to studying the "internal interaction" of the internal AC/DC harmonics of the inverter itself. By deriving the harmonic transfer matrix of the system, the harmonic interaction mechanism on the AC/DC side of the inverter was analyzed, and the conclusion was drawn that harmonic interaction will affect the stability of single-phase grid connected inverters. Reference [9] conducted HSS modeling on a three-phase single L-type filtering inverter, focusing on analyzing the AC/DC harmonic interaction characteristics of the inverter under steady-state conditions [10]. However, the current HSS modeling method can analyze harmonic interactions through the harmonic transfer function matrix, but it has not taken into account the impact of dead zone effects on modeling accuracy and harmonic interaction processes under high switching frequency backgrounds. This will cause certain deviations in the calculation results obtained from HSS modeling and harmonic interaction analysis results.

In order to make the model closer to the actual grid-connected inverter system, this paper analyses the influence of the dead zone effect on the harmonic interaction process of the inverter, and proposes and establishes an improved HSS model to reflect the harmonic interaction principle of the inverter under the dead zone effect. The model takes the dead zone effect into account and quantifies the harmonic interaction coefficient between the inverter and the power grid. The accuracy of the model is verified by theoretical analysis and circuit simulation experiments.

## 2. MODELING OF HSS FOR THREE-PHASE LCL GRID-CONNECTED INVERTER

### 2.1. Harmonic State Space Modeling Principle

The principle of harmonic state space modelling is to decompose a periodic signal in the time domain into multiple harmonic components using Fourier series. These components are then expressed as constants in the frequency domain to avoid complicated time domain calculations. The modelling process assumes that all time-varying signals in the system are periodic signals and constructs the LTP model of the system [11], as shown below:

$$\begin{cases} \dot{x}(t) = \boldsymbol{A}(t)x(t) + \boldsymbol{B}(t)u(t) \\ y(t) = \boldsymbol{C}(t)x(t) + \boldsymbol{D}(t)u(t) \end{cases} \tag{1}$$

The system's state variables, input variables, and output variables are represented by $x(t)$, $u(t)$, $y(t)$ respectively. The state matrix, input matrix, output matrix, and correlation matrix of the system are represented by $\boldsymbol{A}(t)$, $\boldsymbol{B}(t)$, $\boldsymbol{C}(t)$, $\boldsymbol{D}(t)$.

In steady state, the amplitude and phase angle of the time-domain periodically varying signals in the power electronic system remain constant in the frequency domain. To ensure the system equations accurately reflect its dynamic characteristics, we introduce the kernel function $\exp(st)$ and decompose the state, input, and output variables in Eq. (1) into Fourier series. For example, the state variables are decomposed in this way:

$$x(t) = \mathrm{e}^{st} \sum_{n=-\infty}^{+\infty} x_n \mathrm{e}^{jn\omega_1 t} \tag{2}$$

Eq. (2) defines exp(st) as the exponential modulated periodic signal (EMPS), where $x_n$ is the Fourier coefficient of the harmonic of frequency $n$ and $\omega_1$ is the angular frequency. The coefficients of the system, $\boldsymbol{A}(t)$, $\boldsymbol{B}(t)$, $\boldsymbol{C}(t)$ and $\boldsymbol{D}(t)$, remain constant after being converted from the time domain to the frequency domain. By substituting Eq. (2) into Eq. (1), we obtain the following equation:

$$\begin{aligned} \dot{X}(\omega,t) &= A(\omega)\otimes X(\omega,t) + B(\omega)\otimes U(\omega,t) \\ \dot{Y}(\omega,t) &= C(\omega)\otimes X(\omega,t) + D(\omega)\otimes U(\omega,t) \end{aligned} \tag{3}$$

where $\otimes$ is the convolution. Here the convolution in the frequency domain is used to replace the multiplication in the time domain model (3). Simplified according to the harmonic balance principle, the following equation is obtained:

$$\begin{cases} \mathrm{s}\boldsymbol{X} = (\Gamma[\boldsymbol{A}] - \boldsymbol{N})\boldsymbol{X} + \Gamma[\boldsymbol{B}]\boldsymbol{U} \\ \boldsymbol{Y} = \Gamma[\boldsymbol{C}]\boldsymbol{X} + \Gamma[\boldsymbol{D}]\boldsymbol{U} \end{cases} \tag{4}$$

The basic modelling theory of HSS is described in the literature [12, 13], where $X$, $U$ and $Y$ are the forms of the harmonic components of the state, input and output variables, respectively. n is the number of harmonics considered by the model, $\Gamma[\boldsymbol{A}]$ has the form of a Toeplitz matrix, and the specific expansion of $\boldsymbol{X} = \begin{bmatrix} X_{-n} & \cdots & X_{-1} & X_0 & X_1 & \cdots & X_n \end{bmatrix}^{\mathrm{T}}$ is:

$$\Gamma[\boldsymbol{A}] = \begin{bmatrix} A_0 & A_{-1} & \cdots & A_{-n} & 0 & \cdots & 0 & 0 \\ A_1 & A_0 & A_{-1} & \ddots & A_{-n} & 0 & \ddots & 0 \\ \vdots & A_1 & A_0 & A_{-1} & \ddots & A_{-n} & 0 & \vdots \\ A_n & \ddots & A_1 & A_0 & A_{-1} & \ddots & A_{-n} & 0 \\ 0 & A_n & \ddots & A_1 & A_0 & A_{-1} & \ddots & A_{-n} \\ \vdots & 0 & A_n & \ddots & A_1 & A_0 & A_{-1} & \vdots \\ 0 & \ddots & 0 & A_n & \ddots & A_1 & A_0 & A_{-1} \\ 0 & 0 & \cdots & 0 & A_n & \cdots & A_1 & A_0 \end{bmatrix} \tag{5}$$

$N$ is the modulation frequency matrix:

$$\boldsymbol{N} = diag\{-\mathrm{i}n\omega \quad \cdots \quad -\mathrm{i}\omega \quad 0 \quad \mathrm{i}\omega \quad \cdots \quad \mathrm{i}n\omega\} \tag{6}$$

Also, the output calculated through equation (4) is the frequency domain result, which is transformed to the time domain result by the following equation:

$$\begin{aligned} y(t) &= \boldsymbol{T}(t)Y \\ \boldsymbol{T}(t) &= \begin{bmatrix} \mathrm{e}^{-\mathrm{i}n\omega_1 t} & \ldots & \mathrm{e}^{-\mathrm{i}\omega_1 t} & 1 & \mathrm{e}^{\mathrm{i}\omega_1 t} & \ldots & \mathrm{e}^{\mathrm{i}n\omega_1 t} \end{bmatrix} \end{aligned} \tag{7}$$

### 2.2. Inverter HSS Mathematical Model

The mathematical modelling of the three-phase LCL-type grid-connected inverter HSS mathematical model consists of two parts: topology modelling as well as control structure modelling [14], and the two main segments are modelled next, one by one.

## 3. TOPOLOGICAL MODELLING FIGURES.

Three-phase grid-connected LCL inverter topological modelling figures as shown in Fig 1:
In Fig. 1, the input voltage source $e_{\mathrm{dc}}$, the regulator capacitor $C_{\mathrm{dc}}$ and the series resistance $R_{\mathrm{dc}}$ represent the DC side; the right side is the output of the inverter, and the bridge arm side equivalent inductance $L_{\mathrm{i}}$ and resistor $R_{\mathrm{i}}$, the filter capacitor $C_{\mathrm{f}}$ and damping resistor $R_{\mathrm{f}}$, and the network side inductance $L_{\mathrm{g}}$ and resistor $R_{\mathrm{g}}$ represent the AC side, and the AC sense resistor is omitted from the figure.

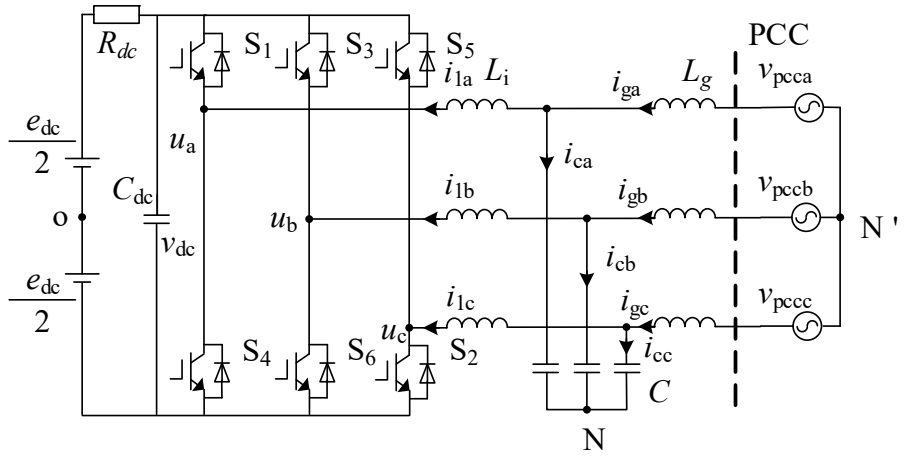


**Fig 1.** Three-phase grid-connected LCL inverter equivalent circuit

According to the inverter equivalent structure diagram shown in Fig. 1, the corresponding system of nonlinear differential circuit equations in the time domain is written as the following equation:

$$\begin{cases} \dfrac{\mathrm{d}i_{\mathrm{lx}}}{\mathrm{d}t} = -\dfrac{R_{\mathrm{i}}+R_{\mathrm{f}}}{L_{\mathrm{i}}}i_{\mathrm{lx}} + \dfrac{R_{\mathrm{f}}}{L_{\mathrm{i}}}i_{\mathrm{gx}} - \dfrac{1}{L_{\mathrm{i}}}v_{\mathrm{fx}} + \dfrac{g_x v_{\mathrm{dc}}}{L_{\mathrm{i}}} \\ \dfrac{\mathrm{d}i_{\mathrm{gx}}}{\mathrm{d}t} = -\dfrac{R_{\mathrm{f}}+R_{\mathrm{g}}}{L_{\mathrm{g}}}i_{\mathrm{gx}} + \dfrac{R_{\mathrm{f}}}{L_{\mathrm{g}}}i_{\mathrm{lx}} - \dfrac{1}{L_{\mathrm{g}}}v_{\mathrm{fx}} + \dfrac{v_{\mathrm{pccx}}}{L_{\mathrm{g}}} \\ \dfrac{\mathrm{d}v_{\mathrm{fx}}}{\mathrm{d}t} = \dfrac{1}{C_{\mathrm{f}}}i_{\mathrm{gx}} - \dfrac{1}{C_{\mathrm{f}}}i_{\mathrm{lx}} \\ \dfrac{\mathrm{d}v_{\mathrm{dc}}}{\mathrm{d}t} = \dfrac{i_{\mathrm{la}}s_{\mathrm{a}} + i_{\mathrm{lb}}s_{\mathrm{b}} + i_{\mathrm{lc}}s_{\mathrm{c}}}{C_{\mathrm{dc}}} - \dfrac{v_{\mathrm{dc}}}{R_{\mathrm{dc}}C_{\mathrm{dc}}} + \dfrac{e_{\mathrm{dc}}}{R_{\mathrm{dc}}C_{\mathrm{dc}}} \end{cases} \tag{8}$$

Where: $i_{\mathrm{g}}$ is the grid-connected side current; $i_{\mathrm{l}}$ is the output bridge arm current; $i_{\mathrm{c}}$ is the filter capacitor current; $v_{\mathrm{dc}}$ is the DC-side regulator capacitor voltage; $v_{\mathrm{pcc}}$ is the point of common coupling (PCC) voltage; $v_{\mathrm{f}}$ is the filter capacitor voltage; and $s_{\mathrm{a}}$, $s_{\mathrm{b}}$, $s_{\mathrm{c}}$ are the three-phase switching functions, respectively. Using small-signal analysis method to linearise the system of equations in Eq. (8), ignoring the components above the second order, a system of linear differential equations can be obtained as shown in Eq. (9).

$$\begin{aligned} i_{\mathrm{dc}}(t) &= i_{\mathrm{la}}(t)s_{\mathrm{a}}(t) + i_{\mathrm{lb}}(t)s_{\mathrm{b}}(t) + i_{\mathrm{lc}}(t)s_{\mathrm{c}}(t) \\ \Delta i_{\mathrm{dc}} &= \mathrm{s}_{\mathrm{ao}}\,\Delta i_{\mathrm{la}} + i_{\mathrm{la}o}\Delta \mathrm{s}_{\mathrm{a}} \\ &\quad + s_{\mathrm{bo}}\Delta i_{\mathrm{lb}} + i_{\mathrm{lb}o}\Delta \mathrm{s}_{\mathrm{b}} \\ &\quad + s_{\mathrm{co}}\Delta i_{\mathrm{lc}} + i_{\mathrm{lco}}\Delta s_{\mathrm{c}} \end{aligned} \tag{9}$$

$$\begin{aligned} g_x &= s_x - \frac{s_{\mathrm{a}} + s_{\mathrm{b}} + s_{\mathrm{c}}}{3} \\ \Gamma[\boldsymbol{G}_x] &= \Gamma[\boldsymbol{S}_x] - \frac{\Gamma[\boldsymbol{S}_{\mathrm{a}}] + \Gamma[\boldsymbol{S}_{\mathrm{b}}] + \Gamma[\boldsymbol{S}_{\mathrm{c}}]}{3} \end{aligned} \tag{10}$$

The small signal (Δ) is used to obtain a small change in switching (Δs) from the controller output. The system of linear differential equations based on linearisation is transformed into harmonic state space equations by HSS modelling through equation (2):

$$\Gamma[\boldsymbol{A}_{\mathrm{t}}]=\begin{bmatrix} -\dfrac{R_{\mathrm{f}}+R_{\mathrm{g}}}{L_{\mathrm{g}}}\boldsymbol{E}_{\mathrm{u}}\text{-}N & -\dfrac{1}{L_{\mathrm{g}}}\boldsymbol{E}_{\mathrm{u}} & \dfrac{R_{\mathrm{f}}}{L_{\mathrm{g}}}\boldsymbol{E}_{\mathrm{u}} & \boldsymbol{Z}_{\mathrm{uv}} \\ \dfrac{1}{C_{\mathrm{f}}}\boldsymbol{E}_{\mathrm{u}} & \boldsymbol{Z}_{\mathrm{uu}}\text{-}N & -\dfrac{1}{C_{\mathrm{f}}}\boldsymbol{E}_{\mathrm{u}} & \boldsymbol{Z}_{\mathrm{uv}} \\ \dfrac{R_{\mathrm{f}}}{L_{\mathrm{i}}}\boldsymbol{E}_{\mathrm{u}} & \dfrac{1}{L_{\mathrm{i}}}\boldsymbol{E}_{\mathrm{u}} & -\dfrac{R_{\mathrm{f}}+R_{\mathrm{i}}}{L_{\mathrm{i}}}\boldsymbol{E}_{\mathrm{u}}\text{-}N & \dfrac{-\Gamma[\boldsymbol{G}]}{L_{\mathrm{i}}} \\ \boldsymbol{Z}_{\mathrm{vu}} & \boldsymbol{Z}_{\mathrm{vu}} & \dfrac{\Gamma[\boldsymbol{S}]}{C_{\mathrm{dc}}} & \dfrac{-\boldsymbol{E}_{\mathrm{v}}}{R_{\mathrm{dc}}C_{\mathrm{dc}}}\text{-}N \end{bmatrix} \tag{11}$$

$$\Gamma[\boldsymbol{B}_{\mathrm{t}}]=\begin{bmatrix} \dfrac{1}{L_{\mathrm{g}}}\boldsymbol{E}_{\mathrm{u}} & \boldsymbol{Z}_{\mathrm{uu}} & \boldsymbol{Z}_{\mathrm{uu}} & \boldsymbol{Z}_{\mathrm{vu}} \\ \boldsymbol{Z}_{\mathrm{uv}} & \boldsymbol{Z}_{\mathrm{uv}} & \boldsymbol{Z}_{\mathrm{uv}} & \dfrac{1}{R_{\mathrm{dc}}C_{\mathrm{dc}}}\boldsymbol{E}_{\mathrm{u}} \end{bmatrix}^{\mathrm{T}} \tag{12}$$

where " $\boldsymbol{E}$ " denotes the unit matrix, " $\boldsymbol{Z}$ " is the zero matrix with the same matrix size as the harmonics under consideration, the subscript t corresponds to the topology and c to the control structure. The multiplication of two time-domain signals can be converted to the frequency domain by means of convolution, obtained as a product of the Toeplitz matrix and the harmonic vectors. The state variables, input variables in the topology are the following vectors:

$$\begin{aligned}\Delta\boldsymbol{X}_{\mathrm{t}}=\big[&\Delta i_{\mathrm{ga}}(t)\quad \Delta i_{\mathrm{gb}}(t)\quad \Delta i_{\mathrm{gc}}(t)\quad \Delta u_{\mathrm{fa}}(t)\quad \Delta u_{\mathrm{fb}}(t)\\ &\Delta u_{\mathrm{fc}}(t)\quad \Delta i_{\mathrm{la}}(t)\quad \Delta i_{\mathrm{lb}}(t)\quad \Delta i_{\mathrm{lc}}(t)\quad \Delta u_{\mathrm{dc}}(t)\big]\end{aligned} \tag{13}$$

$$\Delta\boldsymbol{U}_{\mathrm{t}}=\big[\Delta v_{\mathrm{pcca}}\quad \Delta v_{\mathrm{pccb}}\quad \Delta v_{\mathrm{pccc}}\quad \Delta s_{\mathrm{a}}\quad \Delta s_{\mathrm{b}}\quad \Delta s_{\mathrm{c}}\quad \Delta e_{\mathrm{dc}}\big]^{\mathrm{T}} \tag{14}$$

After establishing the harmonic state space of the topology, the harmonic transfer function matrix corresponding to the topology can be derived from the transfer function equation of the linear state space:

$$\boldsymbol{H}_{\mathrm{t}}(s)=-(\Gamma[\boldsymbol{A}_{\mathrm{t}}]-\boldsymbol{N}_{\mathrm{t}})^{-1}\Gamma[\boldsymbol{B}_{\mathrm{t}}] \tag{15}$$

## 4. MODELLING OF CONTROL STRUCTURES

Modelling of control structures can also be modelled by transforming time domain differential equations to frequency domain differential equations, in this paper the control block diagram is shown in Fig. 2:

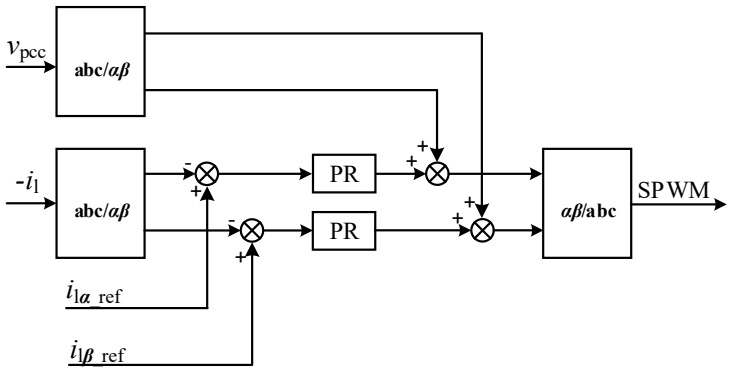


**Fig 2.** Inverter control block diagram

Based on the drawn control block diagram, the corresponding state variables $\boldsymbol{X}_c$, input variables $\boldsymbol{U}_c$, and output variables $\boldsymbol{Y}_c$ in the state space equations of the control structure are selected:

$$\Delta \mathrm{X_c} = \begin{bmatrix} \Delta X_1 & \Delta X_2 & \Delta X_3 & \Delta X_4 \end{bmatrix}^{\mathrm{T}} \tag{16}$$

$$\Delta \boldsymbol{U}_c = \begin{bmatrix} \Delta i_{\alpha\mathrm{ref}} & \Delta i_{\beta\mathrm{ref}} & \Delta i_{\mathrm{la}} & \Delta i_{\mathrm{lb}} & \Delta i_{\mathrm{lc}} & \Delta v_{\mathrm{pcca}} & \Delta v_{\mathrm{pccb}} & \Delta v_{\mathrm{pccc}} \end{bmatrix}^{\mathrm{T}} \tag{17}$$

$$\Delta \boldsymbol{Y}_c = \begin{bmatrix} \Delta s_a & \Delta s_b & \Delta s_c \end{bmatrix}^{\mathrm{T}} \tag{18}$$

In this paper, the current control loop adopts quasi-PR control, and its transfer function and state space equation can be expressed as follows:

$$\mathrm{PR}(s) = k_p + \frac{2k_r\omega_c s}{s^2 + 2\omega_c s + \omega_0^2} \tag{19}$$

Where: $k_p$ is the PR control scaling factor; $k_r$ is the PR control resonance factor; $\omega_0$ is the fundamental frequency; $\omega_c$ is the bandwidth frequency. Let $k_1=k_p$, $k_2=2k_r\omega_c$, $k_3=2\omega_c$, rewriting the control loop into matrix form has:

$$\boldsymbol{A}_c = \begin{bmatrix} Z_{vv} & E_v & Z_{vv} & Z_{vv} \\ -\omega_0^{\,2}E_v & -k_3E_v & Z_{vv} & Z_{vv} \\ Z_{vv} & Z_{vv} & Z_{vv} & E_v \\ Z_{vv} & Z_{vv} & -\omega_0^{\,2}E_v & -k_3E_v \end{bmatrix} \tag{20}$$

$$\boldsymbol{B}_c = \begin{bmatrix} Z_{vv} & Z_{vv} & Z_{vv} & Z_{vv} & Z_{vv} & Z_{vu} \\ E_v & Z_{vv} & \frac{2}{3}E_v & -\frac{1}{3}E_v & -\frac{1}{3}E_v & Z_{vu} \\ Z_{vv} & Z_{vv} & Z_{vv} & Z_{vv} & Z_{vv} & Z_{vu} \\ Z_{vv} & E_v & Z_{vv} & \frac{1}{\sqrt{3}}E_v & -\frac{1}{\sqrt{3}}E_v & Z_{vu} \end{bmatrix} \tag{21}$$

$$\boldsymbol{C}_c = \begin{bmatrix} Z_{vv} & k_2E_v & Z_{vv} & Z_{vv} \\ Z_{vv} & -\frac{k_2}{2}E_v & Z_{vv} & \frac{\sqrt{3}}{2}k_2E_v \\ Z_{vv} & -\frac{k_2}{2}E_v & Z_{vv} & -\frac{\sqrt{3}}{2}k_2E_v \end{bmatrix} \tag{22}$$

$$\boldsymbol{D}_c = \begin{bmatrix} k_1E_v & Z_{vv} & & \\ -\frac{k_2}{2}E_v & \frac{\sqrt{3}}{2}k_1E_v & k_1M & M \\ -\frac{k_2}{2}E_v & -\frac{\sqrt{3}}{2}k_1E_v & & \end{bmatrix} \tag{23}$$

$$\boldsymbol{M} = \begin{bmatrix} \frac{2}{3}E_v & -\frac{1}{3}E_v & -\frac{1}{3}E_v \\ -\frac{1}{3}E_v & \frac{2}{3}E_v & -\frac{1}{3}E_v \\ -\frac{1}{3}E_v & -\frac{1}{3}E_v & \frac{2}{3}E_v \end{bmatrix} \tag{24}$$

The control structure state space equations are obtained from the derived matrices of the coefficients:

$$\begin{aligned} \Delta\dot{\boldsymbol{X}}_{\mathrm{c}} &= \boldsymbol{A}_{\mathrm{c}}\Delta\boldsymbol{X}_{\mathrm{c}} + \boldsymbol{B}_{\mathrm{c}}\Delta\boldsymbol{U}_{\mathrm{c}} \\ \Delta\boldsymbol{S} &= \boldsymbol{C}_{\mathrm{c}}\Delta\boldsymbol{X}_{\mathrm{c}} + \boldsymbol{D}_{\mathrm{c}}\Delta\boldsymbol{U}_{\mathrm{c}} \end{aligned} \tag{25}$$

The same process of derivation of the state space equations of the topological structure leads to the matrix of harmonic transfer functions of the control structure:

$$\boldsymbol{H}_{\mathrm{c}}(s) = \Gamma[\boldsymbol{C}_{\mathrm{c}}](-\Gamma[\boldsymbol{A}_{\mathrm{c}}] + \boldsymbol{N}_{\mathrm{c}})^{-1}\Gamma[\boldsymbol{B}_{\mathrm{c}}] + \Gamma[\boldsymbol{D}_{\mathrm{c}}] \tag{26}$$

### 4.1. Inverter HSS Modelling with Dead-zone Effect

As stated in the introduction, the current research on HSS modelling of inverters does not consider the impact of dead time effects on the modelling accuracy and the interaction process. Although the percentage of dead time in the switching cycle is very small, with the current trend of higher and higher switching frequency, the accumulation of low harmonics caused by the dead time effect results in more serious distortion of the output waveforms and errors in the harmonic interaction coefficients. Therefore, in order to accurately analyse the harmonic interaction of the inverter, this paper considers the deadband effect into the three-phase inverter HSS modelling process, and analyses the impact of the deadband effect on the harmonics and the coupling relationship of the inverter variables.

## 5. ANALYSIS OF DEAD-ZONE EFFECTS

In a bridge inverter, a dead time must be inserted between complementary drive signals in order to prevent "pass-through" between the upper and lower switching devices of the same bridge arm [15]. Before adding the dead time effect to the HSS modelling process, a dead time effect analysis is required to quantify the specific impact of the dead time effect on the inverter. Let the inverter bridge arm current i1 flow to the grid-connected point when $i_1$>0, and vice versa when $i_1$<0. When $i_1$ flows to the grid-connected point, the inverter bridge arm voltage and the switching device drive voltage signals are shown in Fig. 3:

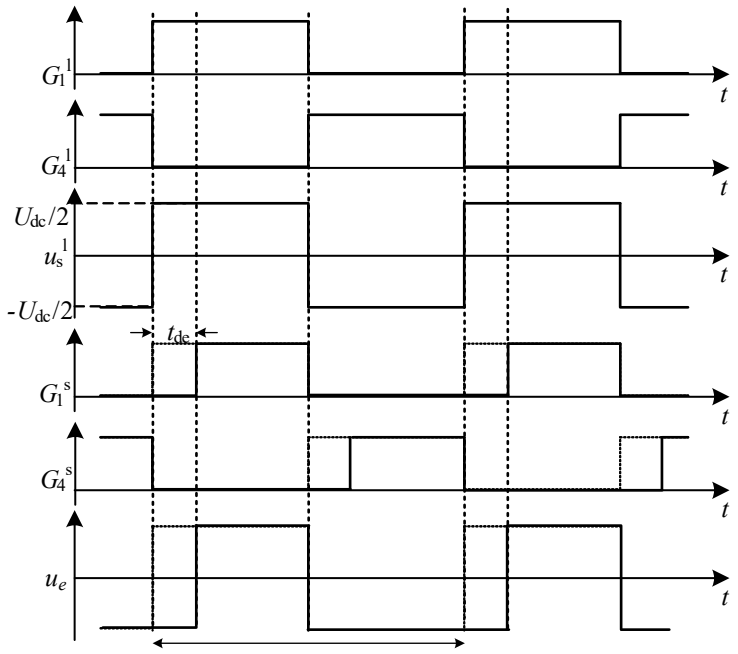


**Fig 3.** Output voltage waveform under dead zone effect

In Fig. 3: $t_{de}$ is the dead time; T is the switching period; ton and toff are the device on and device off delays; $G_1^1$ and $G_4^1$ are the ideal drive signal waveforms of the switching tubes T1 and T4,

respectively, and $G_1^s$ and $G_4^s$ are the actual drive signal waveforms of the switching tubes T1 and T4 after the addition of the dead effect, respectively. $u_s^1$ is the ideal output voltage signal of the inverter, and $u_e^1$ is the actual output voltage signal of the inverter. ideal output voltage signal of the inverter, ue is the actual output voltage signal of the inverter.

In the existing studies, the deadband effect is equivalent to superimposing an error voltage with constant amplitude and direction determined by the direction of the output current of the bridge arm on the output voltage terminal of the inverter bridge. In order to quantify the influence of non-ideal factors on the inverter output voltage, the error voltage caused by the deadband effect and the non-ideal characteristics of the device is derived step by step through the equation as shown in Eq. (27):

$$v_{de} = U_{e1}\text{sign}(i_l) \tag{27}$$

$$U_{el} = -2U_{dc}t_{de} / T_S;\text{sign}(i_l) = \begin{cases} 1, & i_l > 0 \\ -1, & i_l < 0 \end{cases} \tag{28}$$

In the actual circuit, the deadband effect error voltage coefficient $D_{de}$ and the deadband error voltage $v_{de}$ are derived as shown in equation 29:

$$D_{de} = \frac{-2t_d\text{sign}(i_l)}{T_S};v_{de} = D_{de}U_{dc} \tag{29}$$

## 6. IMPROVED MODELLING OF INVERTER HSS WITH DEAD-ZONE EFFECT

With the deadband error voltage obtained from the derivation in the previous section, in order to incorporate the deadband effect into the HSS modelling, the following improvements are made to the formulae in the set of linear differential equations for the output voltage of the bridge arm during the modelling process:

$$\begin{aligned} \frac{\mathrm{d}i_{cx}}{\mathrm{d}t} &= \frac{R_2}{L_c}i_{gx} - \frac{R_2}{L_c}i_{cx} + \frac{1}{L_c}v_{fx} - \frac{g_x v_{dc} + v_{de}}{L_c} \\ &= \frac{R_2}{L_c}i_{gx} - \frac{R_2}{L_c}i_{cx} + \frac{1}{L_c}v_{fx} - \frac{(g_x + D_{de})v_{dc}}{L_c} \end{aligned} \tag{30}$$

According to the improved set of differential equations, the matrix refinement of the HSS modelling process, the deadband voltage error coefficients are similarly transformed from the multiplication form in the time domain to the convolution under the frequency domain by Fourier transform and written into the state coefficients matrix $\Gamma[\boldsymbol{A}_t]$ by changing the Toeplitz matrix into the form of $\Gamma[D_{de}]$ as shown in Equation (31):

$$\Gamma[\boldsymbol{A}_t] = \begin{bmatrix} -\frac{R_f + R_g}{L_g}\boldsymbol{E}_u\text{-}N & -\frac{1}{L_g}\boldsymbol{E}_u & \frac{R_f}{L_g}\boldsymbol{E}_u & \boldsymbol{Z}_{uv} \\ \frac{1}{C_f}\boldsymbol{E}_u & \boldsymbol{Z}_{uu}\text{-}N & -\frac{1}{C_f}\boldsymbol{E}_u & \boldsymbol{Z}_{uv} \\ \frac{R_f}{L_i}\boldsymbol{E}_u & \frac{1}{L_i}\boldsymbol{E}_u & -\frac{R_f + R_i}{L_i}\boldsymbol{E}_u\text{-}N & \frac{-\Gamma[\boldsymbol{G}] - \Gamma[\boldsymbol{D}_{de}]}{L_i} \\ \boldsymbol{Z}_{vu} & \boldsymbol{Z}_{vu} & \frac{\Gamma[\boldsymbol{S}]}{C_{dc}} & \frac{-\boldsymbol{E}_v}{R_{dc}C_{dc}}\text{-}N \end{bmatrix} \tag{31}$$

# 7. INVERTER HARMONIC INTERACTION ANALYSIS

In the HSS modelling approach, the time-domain period-varying components are transformed into complex frequency-domain constants, and each variable involved in the modelling contains information on all harmonics up to the *n* order under consideration. In contrast to the traditional LTI system, which can only consider the corresponding transmission relationship between variables of the same frequency, the HSS modelling, as an LTP system, incorporates the coupling influences between variables of different frequencies into the modelling process, and quantifies the coupling relationship between the input variables and the output variables of different frequencies through the derivation of the harmonic transmission coupling matrices at the LTP system.

## 7.1. Inverter Transfer Function Matrix with Dead-zone Effect

Inverter transfer function matrix with dead-zone effect $\boldsymbol{H}_z(s)$ need to be used by the above has been derived from the topology and the control structure of the transfer function matrix, the two through the relationship between the input and output variables for the union of the simplified is the overall transfer function matrix of the system [16], and due to the limitation of the space in this paper, only the logic diagram of the relationship between the two mergers is given, as shown in Fig. 4:

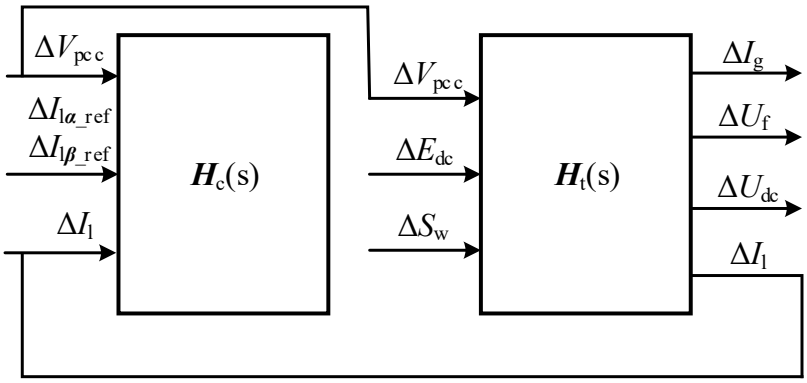


**Fig 4.** Combined diagram of the overall transfer function of the system

The transfer function matrix of the system as a whole after combining the two associatively is shown in Eq. (32), and the interaction coefficients between the input variables and the output variables at each frequency on both sides of the equation can be quantified by $\boldsymbol{H}_z(s)$, and the magnitude of the interaction coefficients can be analysed to reflect the degree of coupling between a certain harmonic of the input variable and a certain frequency harmonic of the output variable:

$$\begin{bmatrix} \Delta I_g \\ \Delta V_f \\ \Delta I_l \\ \Delta V_{dc} \end{bmatrix} = \boldsymbol{H}_z(s) \begin{bmatrix} \Delta I_{l\alpha-ref} \\ \Delta I_{l\beta-ref} \\ \Delta V_{pcc} \\ \Delta E_{dc} \end{bmatrix} \tag{32}$$

# 8. SIMULATION ANALYSIS

According to the modelling process in the previous section, the harmonic analysis of the HSS model is implemented in Matlab by writing a program and outputting the calculation results. At the same time, the simulation model of three-phase grid-connected inverter with the same parameters is built in Simulink. Next, the simulation analysis of the established HSS improvement model of the inverter under the dead zone effect is carried out, and two parts of comparison experiments are mainly conducted: time domain validation and harmonic interaction analysis of the inverter. The time-domain validation can verify the accuracy of the improved HSS model considering the deadband

effect, while the inverter harmonic interaction analysis can visually quantify the degree of influence of the deadband effect on the whole harmonic interaction process.

## 8.1. Time-domain Validation

The time domain validation is to compare the calculation results of the HSS model built in Matlab by writing the program with the output results of the three-phase grid-connected inverter simulation model constructed in Simulink, to judge the difference between the waveforms of the two in the time domain and the amplitude of each harmonic in the frequency domain, and to validate the accuracy and reliability of the built HSS model, with the specific parameters shown in Table 1.

**Table 1.** Simulate specific parameters

| parameter | value | parameter | value |
|---|---|---|---|
| Grid-side inductance $L_g$/mH | 0.4 | DC Side Voltage Source $e_{dc}$/V | 725 |
| Grid-side resistance $R_g$/Ω | 1e-3 | Voltage regulator capacitors $C_{dc}$/μf | 100 |
| Filter capacitor $C_f$/μf | 100 | DC Side Resistance $R_{dc}$/Ω | 1e-3 |
| Damping Resistors $R_f$/Ω | 1e-3 | PR control scale factor $k_p$ | 3.3 |
| Bridge arm side inductor$L_i$/mH | 1.8 | PR control bandwidth frequency $\omega_c$/rad. $s^{-1}$ | 60.5 |
| Bridge arm side resistance $R_i$/Ω | 1e-3 | PR control resonance factor $k_r$ | 10 |
| switching frequency fs/Hz | 10k | dead time $t_{de}$/s | 2e-6 |

The HSS model considering the dead zone effect and the three-phase grid-connected inverter simulation model is established with the above parameters. Next, the HSS model is validated in the time domain by comparing the grid-connected current with the DC measured voltage, and the results are shown in Fig. 5 and Fig. 6:

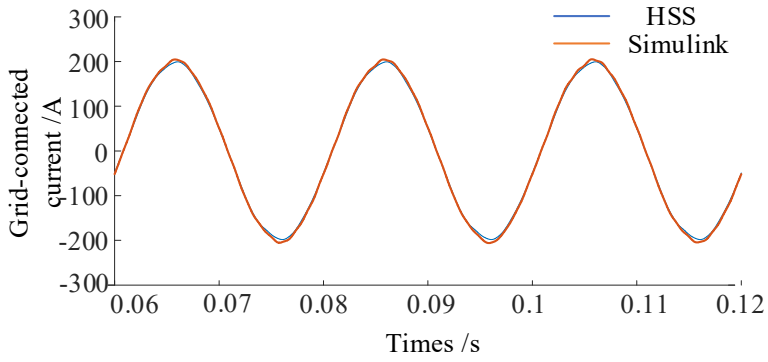


**Fig 5.** Plot of grid-connected current in time domain vs. frequency domain

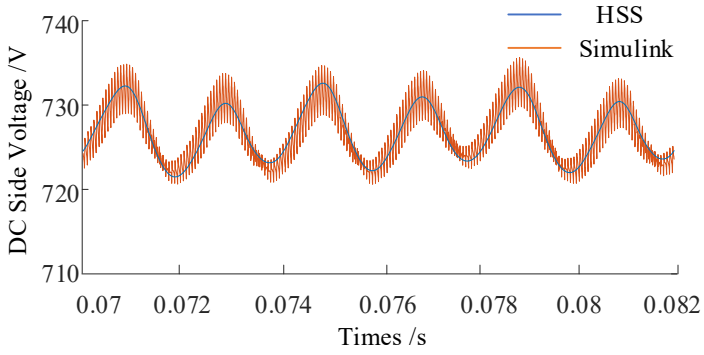


**Fig 6.** DC side voltage time domain vs. frequency domain plot

Table 2 gives the values of the simulation operation and HSS calculation in the frequency domain of the grid-connected current, and comparing the specific amplitude of each harmonic in the frequency domain of the two, it is found that the error of the calculated value of the HSS model is less than 1%. It can be seen that the calculated results of the HSS model with the addition of the dead zone effect of device switching are in good agreement with the time-domain results given by the simulation model in Simulink, which verifies the accuracy of the calculated results of the HSS model.

**Table 2.** Grid-connected current simulation and HSS harmonic output results

| Harmonic frequency of grid-connected current | simulated value | HSS calculated value |
|---|---|---|
| 1 | 200.02 | 200.02 |
| 3 | 0.022434161 | 0.024378193 |
| 5 | 1.706485109 | 1.773125269 |
| 7 | 1.438871058 | 1.449628777 |
| 9 | 0.014856603 | 0.029091782 |
| 11 | 0.200373827 | 0.130261745 |

## 8.2. Harmonic Interaction Analysis

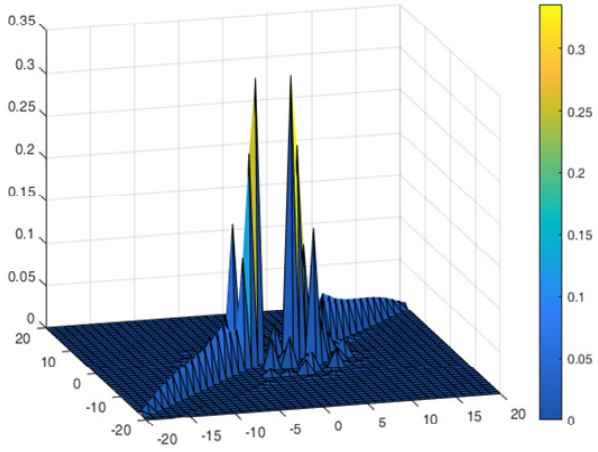


**Fig 7.** Ideal harmonic coupling admittance diagram

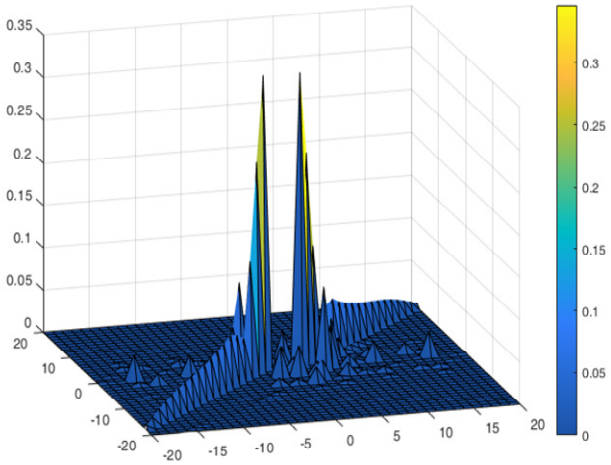


**Fig 8.** Harmonic coupling admittance diagram under dead zone effect

The harmonic interaction analysis is performed by comparing the overall transfer function matrix $\boldsymbol{H}_z(s)$ of the system derived in subsection 3. 1, analysing the coupling relationship between the input and output variables corresponding to each frequency on both sides of the matrix and analysing and quantifying the relationship through the matrix,, and the coupling coefficients of the grid-connected current $i_{ga}$ and the grid-connected voltage $v_{pcca}$ with or without the addition of dead zone effect are given in the schematic diagrams for the purpose of analysing the specific impact of the dead zone effect on the harmonic coupling relationship.

Figs. 7 and 8, it can be clearly observed that the interaction between the grid-connected current $i_{ga}$ and the grid-connected voltage $v_{pcca}$ becomes more complicated after considering the dead-zone effect of the device switching, and the interaction between the harmonics of each frequency and the interaction near the fundamental frequency is mainly increased. The difference of the collected data can be obtained in Table 3:

**Table 3.** The difference of the interaction coefficient under non-ideal factors

| Frequency of grid-connected currents | Frequency of grid-connected voltages | Difference in interaction coefficients |
|---|---|---|
| 3 | 1 | 0.007916 |
| 5 | 1 | 0.030034 |
| 7 | 1 | 0.0201923 |
| 11 | 1 | 0.0014044 |
| 13 | 1 | 0.0016019 |
| 5 | 7 | 0.0005912 |
| 7 | 9 | 0.0003704 |

According to the graph, the main effects of the dead zone effect after the addition of the grid current 5, 7, 11, 13 frequency harmonics and grid voltage fundamental wave interaction, resulting in grid current 5, 7, 11, 13 frequency harmonics content of the increase, and then increased the interaction between the grid current and the grid voltage odd harmonics, but the degree of increase is lower than the odd harmonics and the interaction between the fundamental wave. The comparison of the amplitude of each frequency harmonic in the frequency domain of the grid-connected current before and after adding the dead zone effect is shown in Fig. 9:

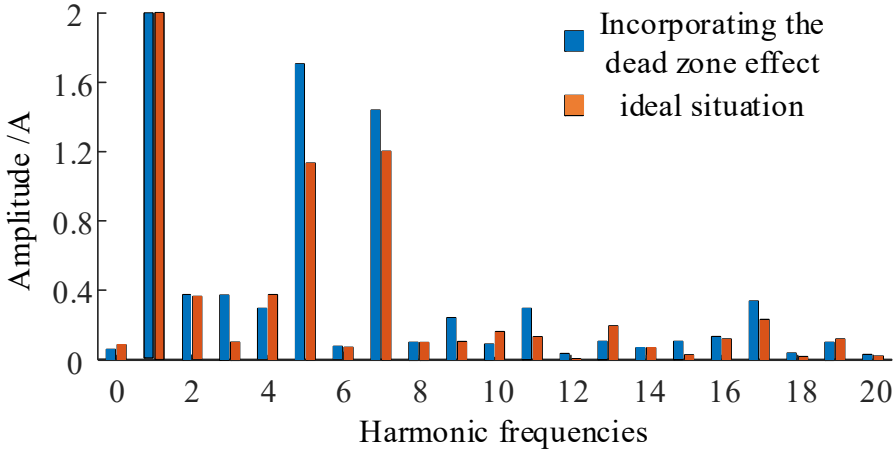


**Fig 9.** Comparison diagram of grid-connected current before and after adding dead zone effect

Comparison reveals that there is a significant increase in the harmonic content of the grid-connected currents at frequencies 5, 7, 11, and 13 after the deadband effect is added, which is in line with the interaction effect relationship derived from the harmonic transfer function matrix.

Subsequently, the switching frequency and dead time are changed for comparison experiments, and the results are shown in Table 4. Comparing the simulated output waveform distortion rate and the calculated waveform distortion rate of HSS, although there is an error between the two, the error is very small and it can be concluded that the improved HSS model after adding the deadband effect is accurate and effective. Then, comparing the results of experiments 1, 2 and 3, it is observed that with the increase of dead time, the dead time effect on the distortion rate of the grid-connected current and the harmonic interaction between the grid-connected current and the grid-connected voltage deepens under the same switching frequency. On the other hand, comparing the results of groups 2, 4 and 6 corresponding to the distortion rate and the interaction coefficient between the fifth harmonic of the grid current and the fundamental wave of the grid voltage, it can be seen that the deadband effect deepens the influence on the distortion rate of the grid current and the interaction between the grid current and the harmonics of the grid voltage with the increase of switching frequency under the same switching cycle ratio.

**Table 4.** Harmonic interaction coefficients at different dead times

| Experimental group number | Switching frequency | dead time /μs | Simulated waveform distortion rate/% | HSS waveform distortion rate/% | $Y_{ig5\text{-}vp}$ |
|---|---|---|---|---|---|
| 1 | 10kHz | 1 | 2.83 | 2.94 | 0.017456 |
| 2 | | 2 | 2.91 | 3.07 | 0.030034 |
| 3 | | 5 | 3.48 | 3.78 | 0.0478355 |
| 4 | 20kHz | 1 | 3.04 | 3.46 | 0.0354626 |
| 5 | | 2 | 3.31 | 3.69 | 0.0384656 |
| 6 | 50kHz | 0.4 | 3.25 | 3.44 | 0.0362544 |
| 7 | | 2 | 5.62 | 6.18 | 0.0553258 |

$Y_{ig5\text{-}vp}$ in the table. 4 indicates the interaction difference between the fifth harmonic of the grid-connected current and the fundamental of the grid-connected voltage.

## 9. SUMMARY

This paper proposes and establishes an improved inverter HSS mathematical model considering the dead zone effect, which makes up for the defects of the traditional HSS model ignoring the dead zone effect, so that the established system model is closer to the actual system. And through the derivation of the system transfer function matrix, the influence of the dead zone effect on the interaction coefficient of the inverter is quantitatively analysed, and the following conclusions are drawn based on the theoretical analysis and simulation verification:

1) By establishing the HSS model of the grid-connected inverter considering the dead zone effect, and comparing the frequency-domain simulation value of the grid-connected current and the calculated value of the HSS, it is found that the error of the calculated value of the HSS model is less than 1%, and the time-domain waveforms of both of them are very consistent, which verifies the accuracy of the calculation results of the HSS model.

2) By deriving the system transfer function matrix, it is concluded that the dead time leads to an increase in the 5th, 7th, 11th and 13th frequency harmonic content in the grid-connected current, which in turn affects the degree of interaction of odd harmonics between the grid-connected current

and the grid voltage. As the dead time and the switching frequency increase, the resulting effect intensifies

# REFERENCES


[1] WANG Jinning, WANG Lei, HAN Xiaoqing, et al. Analysis on AC/DC Harmonic Coupling Characteristics of Converter Based on Harmonic State Space Modeling [J]. Power System Automation, 2020, 44(04):159-167.

[2] LIN Shun-Fu, DAI Ye-Min, YAN Xin-Yu et al. Distributionally robust optimal dispatching of integrated ene-rgy system considering line pack effect of gas network [J]. Power Automation Equipment, 2022, 42(06):76-83. DOI:10. 16081/j. epae. 202203015.

[3] ZHOU Yan, LI Xianyun, WANG Shuzheng. Harmonic State Space Modeling and Analysis of Direct Current Distributi on Network [J]. Power Electronics Technology, 2022, 56(02):91-96.

[4] XU Dezhi, WANG Fei, MAO Hualong, et al. Modeling and Analysis of Harmonic Interaction Between Multiple Grid-connected Inverters and the Utility Grid [J]. Chinese Journal of Electrical Engineering, 2013, 33(12):64-71.

[5] ZHU Ting, HU Haitao, TAO Haidong. Three-phase VSC frequency coupling admittance modelling and harmonic characteristics analysis based on HSS [J]. Journal of Electrical Machines and Control, 2022, 26(03):78-86. DOI:10. 15938/j. emc. 2022. 03. 009.

[6] ZHANG Guorong, GAO Kai, XIE Runsheng, et al. Modeling and analysis of grid-connected inverter considering AC and DC harmonic coupling [J/OL]. Electrical Measurement and Instrumentation: 1-9[2024-04-09]. http: //kns. cnki. net/kcms/detail/23. 1202. TH. 20210729. 1333. 004. html.

[7] ZHANG Guorong, XU Chenlin, CAI Zhibin, et al. A modeling method for a converter based on harmonic state space [J]. Power System Protection and Control, 2021, 49(11):141-147. DOI:10. 19783/j. cnki. pspc. 200958.

[8] D. G. Infield, P. Onions, A. D. Simmons, and G. A. Smith, “Power quality from multiple grid-connected single-phase inverters, ” IEEE Trans. Power Del. , vol. 19, no. 4, pp. 1983–1989, Oct. 2004.

[9] WANG Fei, FENG Xiayun, WU Chunhua, et al. Study on harmonic interaction of multiple-flyback microinverters for grid-connection [J]. Chinese Journal of Electrical Engineering, 2016, v. 36;No. 542(03):125-132.

[10] XIE Ning, LUO An, CHEN YanDong, et al. Dynamic modelling and harmonic characterization of large-scale photovoltaic power plants[J]. Chinese Journal of Electrical Engineering, 2013, 14(36):10-17.

[11] CHEN Xin, ZHANG Chang, WANG ZanCheng. Study on the dynamic interaction effects between photovoltaic grid-connected inverter and power grid based on impedance analysis[J]. Chinese Journal of Electrical Engineering, 2014, 34(27):4559-4567.

[12] Z. Xu et al. , “A Complete HSS-Based Impedance Model of MMC Considering Grid Impedance Coupling, ” IEEE Trans. Power Electron. , vol. 35, no. 12, pp. 12929–12948, Dec. 2020, doi: 10. 1109/TPEL. 2020. 2996714.

[13] J. Kwon, X. Wang, F. Blaabjerg, C. L. Bak, V. -S. Sularea, and C. Busca, “Harmonic Interaction Analysis in a Grid-Connected Converter Using Harmonic State-Space (HSS) Modeling, ” IEEE Trans. Power Electron. , vol. 32, no. 9, pp. 6823–6835, Sep. 2017, doi: 10. 1109/TPEL. 2016. 2625802.

[14] G. N. Love and A. R. Wood, “Harmonic State Space model of power electronics, ” in 2008 13th International Conference on Harmonics and Quality of Power, Wollongong, NSW: IEEE, Sep. 2008, pp. 1–6. doi: 10. 1109/ ICHQP. 2008. 4668792.

[15] Y. Cai, Y. He, H. Zhang, H. Zhou, and J. Liu, “Research on Harmonic State-Space Modeling and Calculation Analysis of Low-Switching-Frequency Grid-Connected Inverter Considering the Impact of Digitization, ” IEEE Trans. Power Electron. , vol. 38, no. 1, pp. 1003–1021, Jan. 2023, doi: 10. 1109/TPEL. 2022. 3201626.

[16] D. G. Infield, P. Onions, A. D. Simmons, and G. A. Smith, “Power quality from multiple grid-connected single-phase inverters,” IEEE Trans. Power Del. , vol. 19, no. 4, pp. 1983-1989, Oct. 2004.